Progress in Reaction Kinetics and Mechanism

ARTICLE

Open Access

https://doi.org/10.48130/prkm-0026-0014

Progress in Reaction Kinetics and Mechanism **2026**, 51: e022

Pyrolysis kinetics and backbone decomposition mechanisms of nylon 6/6: insights from TG-FTIR-GC/MS and density functional theory

Donghua Xu, Haoyu Xiao, Shengwei Feng, Yingquan Chen, Xianhua Wang, Hanping Chen and Haiping Yang*

State Key Laboratory of Coal Combustion, School of Energy and Power Engineering, Huazhong University of Science and Technology, 1037 Luoyu Road, Wuhan, Hubei 430074, China

* Correspondence: yhping2002@163.com (Yang H)

Abstract

A limited understanding of the pyrolysis mechanisms hinders the efficient thermochemical conversion and recovery of nylon waste. This study investigates the pyrolysis behavior, volatile evolution, and backbone degradation mechanisms of nylon 6/6 by integrating thermogravimetry-Fourier transform infrared spectroscopy-gas chromatography/mass spectrometry (TG-FTIR-GC/MS) and density functional theory (DFT) calculations. According to TG analysis, nylon 6/6 undergoes pyrolysis mainly in the range of 390–515 °C, with a mass loss of 95.86 wt%, and exhibits the most intense degradation at approximately 480 °C. Kinetic analysis using the Coats-Redfern integral and Achar differential methods indicates that nylon 6/6 pyrolysis follows the first-order reaction model with an apparent activation energy of 278 kJ/mol. Online FTIR and offline GC/MS identify the characteristic gaseous products, including CO_2, NH_3, 1-amino-5-hexene (13.54%), and cyclopentanone (79.64%). Furthermore, DFT calculations elucidate the electrostatic potential (ESP) distribution, Fukui function indices, and bond dissociation energies (BDEs) of the nylon 6/6 model molecule. Results demonstrate that the nucleophilic attack of the terminal amino group and the free radical attack of H· facilitate the cleavage of the amide structure. The generated hexamethylenediamine and adipic acid segments subsequently undergo deamination and cyclization reactions to form 1-amino-5-hexene and cyclopentanone, respectively. By elucidating the backbone degradation mechanisms and product formation pathways during nylon 6/6 pyrolysis, the multi-scale study provides a theoretical basis for the recovery of high-value fuels and chemicals from nylon waste.

Keywords: Nylon 6/6, Pyrolysis, TG-FTIR-GC/MS, Density functional theory, Fukui function

Citation: Xu D, Xiao H, Feng S, Chen Y, Wang X, et al. 2026. Pyrolysis kinetics and backbone decomposition mechanisms of nylon 6/6: insights from TG-FTIR-GC/MS and density functional theory. *Progress in Reaction Kinetics and Mechanism* 51: e022 https://doi.org/10.48130/prkm-0026-0014

Introduction

Polyamide (also known as nylon), an essential engineering plastic, is renowned for its superior mechanical strength, thermal stability, and chemical resistance, leading to widespread applications in textiles, automotive, and electronics industries, with global production continuously rising[1]. Nevertheless, the durability of nylon contributes to significant post-consumer waste accumulation, posing serious environmental risks such as microplastic pollution and the release of harmful substances. Conventional disposal methods like incineration and landfilling are not only economically inefficient but also contribute to carbon emissions and potential soil and water contamination. Mechanical (physical) recycling often results in downgraded material quality due to polymer chain scission during reprocessing, limiting the application of recycled products[2,3]. Consequently, developing advanced valorization techniques is crucial for achieving high-value recycling of nylon waste, mitigating environmental impact, and promoting a circular plastic economy.

Pyrolysis has emerged as a promising technology for recovering value-added fuels, chemicals, and functional carbon materials from plastic waste through deep cracking of polymers in an oxygen-limited environment[4,5]. For instance, Xiao et al. reported that using polypropylene (PP) pyrolysis volatiles as a carbon source, catalytic reforming over ZSM-5 at a medium temperature (400 °C) enabled the highly selective production of BTX (benzene, toluene, and xylene)[6], while chemical vapor deposition on Fe/Al_2O_3 catalyst at a high temperature (800 °C) could produce valuable carbon nanotubes and hydrogen[7]. Based on a temperature-gradient pyrolysis strategy, Munyaneza et al.[8] efficiently recycled α-olefins from polyethylene (PE). Additionally, Sukkasem et al.[9] utilized a low-cost agricultural-waste-derived SUZ-4 zeolite to transform polystyrene (PS) into 81.60 wt% oil with 70.56% selectivity toward mono-aromatic hydrocarbons. However, most previous studies have predominantly focused on polyolefin plastics with simple elemental composition, paying insufficient attention to heteroatom-containing plastics. The long-term persistence of nylon in real-world plastic waste streams introduces significant challenges. During pyrolysis, the decomposition of amide groups in nylon waste releases substantial nitrogen-containing compounds, which not only poison catalysts, reduce process efficiency, and increase energy consumption but also negatively affect product composition, leading to compromised stability in downstream applications[10]. For example, the pyrolysis of composite packaging waste (nylon 6 and PE) generated a large number of nitrogen-containing volatiles, resulting in a significant increase in the acidity of pyrolytic oil[11]. Similarly, a study demonstrated that incorporating nylon polymer into the feedstock resulted in the pyrolytic oil with nitrogen content significantly exceeding fuel standards.[12] Furthermore, these nitrogen-containing components preferentially occupied the acidic sites of catalysts, significantly reducing deoxygenation efficiency[13]. Besides, Kumagai et al.[14] discovered that HCN formation during polyimide pyrolysis substantially degraded syngas quality. These adverse impacts of nitrogen-containing compounds fundamentally stem from an inadequate understanding of the pyrolysis

https://doi.org/10.48130/prkm-0026-0014

mechanisms of nylon waste[15]. Therefore, revealing the pyrolysis characteristics and backbone degradation pathways of nylon is crucial for suppressing the formation of nitrogen-containing by-products and achieving its clean and efficient utilization.

The combination of thermogravimetry-Fourier transform infrared spectroscopy (TG-FTIR) and pyrolysis-gas chromatography/mass spectrometry (Py-GC/MS) has been widely employed to investigate the pyrolysis mechanisms of nitrogen-containing polymers. This approach enables real-time monitoring of the mass loss of raw materials and the release of gaseous volatiles[16]. By integrating TG-FTIR and Py-GC/MS, Liu et al.[3] investigated the co-pyrolysis of textile waste with red mud, elucidating the release patterns of nitrogen-containing volatiles and their impact on the catalyst. Zheng et al.[17] revealed the evolution of C–N functional groups and determined the kinetic parameters for distinct pyrolysis stages during the pyrolysis of polyurethane foam. However, TG-FTIR typically employs slow and controlled heating rates, whereas Py-GC/MS often uses instantaneous flash pyrolysis. This inconsistency may lead to deviations between the detection results obtained from FTIR and those from GC/MS. In contrast, the integration of these techniques into a single TG-FTIR-GC/MS system enables the comprehensive characterization of pyrolysis products under a unified heating program. This coupled system allows for the direct transfer of released volatiles from the TG to both the FTIR for online analysis of functional groups and the GC/MS for efficient separation and identification of volatile components at specific temperatures. Nevertheless, due to the limitations of detection sensitivity and temporal resolution, experimental methods struggle to capture short-lived and highly reactive free radicals and nitrogen-containing intermediates, which are particularly crucial for elucidating the pyrolysis mechanisms of nylon[10]. By computing the electronic properties of organic compounds, density functional theory (DFT) can provide key microscopic thermodynamic and kinetic parameters, thereby enabling prediction of chemical bond cleavage at the atomic level and elucidation of the formation mechanisms of pyrolytic intermediates and products[18]. Numerous studies have successfully employed DFT as a powerful complement to experimental methods, clarifying the pyrolysis mechanisms of polymers such as PE, polypropylene (PP), and polyethylene terephthalate (PET) through calculations of bond dissociation energies (BDEs), demonstrating the value of DFT in polymer pyrolysis research[19–21]. Nevertheless, unlike these polymers, the amide groups in nylon chains exhibit conjugation effects and form strong intermolecular hydrogen-bonding networks, which can significantly alter the energy barriers for backbone scission. This leads to multiple competing degradation pathways that cannot be reliably predicted by simple BDE ranking alone. For instance, in a DFT study on a nylon 6 model molecule, Wang et al.[19] discovered that the C–N bond in the amide group showed a high BDE, making its direct cleavage unlikely. Thus, relying solely on BDE cannot explain the formation of caprolactam, a key monomer product. Given that nylon chains contain reactive terminal amino and carboxyl groups, their degradation likely involves cooperative reactions initiated by these active sites. Therefore, understanding the micro-scale reactivity of nylon molecules requires an integrated assessment based on multiple parameters such as charge distribution, BDEs, and Fukui functions. In summary, establishing a multi-scale analytical framework that synergistically combines macro-scale experimental data from TG-FTIR-GC/MS with microscale theoretical simulations from DFT is particularly critical for elucidating the pyrolysis mechanism of nylon. Such an integrated approach can systematically reveal the competing reaction pathways, clarify the formation mechanisms of characteristic nitrogen-containing products, and ultimately provide fundamental insights for optimizing the pyrolysis of nylon waste, enabling targeted control over reaction pathways and enhancing the value of the final products.

Nylon 6/6 was selected for this study due to its high production volume and extensive application, its representativeness in the nylon family enabling extrapolation of findings, and the existing knowledge gap regarding its pyrolysis mechanisms that this research aims to address[3]. The mass loss characteristics of nylon 6/6 were first examined via TG analysis, with apparent kinetic calculations. Subsequently, the released gaseous products were monitored in real-time through FTIR, and the volatile components were precisely identified employing GC/MS, enabling the correlation of specific pyrolysis stages with the release profiles of volatiles. Finally, DFT calculations were performed to determine the key microscopic descriptors of the nylon 6/6 model molecule, including electrostatic potential (ESP) distribution, condensed Fukui functions, and BDEs. This integrated approach, combining macroscopic experimental data with microscopic theoretical simulations, is anticipated to provide comprehensive insights into the pyrolysis behavior, product evolution, and backbone cracking mechanisms of nylon 6/6, thereby establishing a fundamental basis for optimizing its pyrolysis process towards high-value utilization.

Materials and methods

Materials

Nylon 6/6 (CAS 32131-17-2) was purchased from Aladdin Biochemical Technology Co., Ltd (Shanghai, China). As shown in Fig. 1a, nylon 6/6 is a polyamide synthesized from hexamethylenediamine and adipic acid, characterized by its symmetrical repeating unit with amide groups (–NH–CO–) oriented in alternating directions. This structural regularity enables strong intermolecular hydrogen bonding, contributing to high mechanical strength and thermal stability[22]. In contrast, another common nylon polymer, nylon 6 (polycaprolactam), is derived from caprolactam monomers, resulting in unidirectional amide bonds and less symmetrical chain alignment[23]. The characteristic functional groups of nylon 6/6 were analyzed using an FTIR spectrometer (Nicolet iS50R, Thermo Fisher, USA), as presented in Fig. 1b. The absorption peaks at 3,294 and 1,537 cm^{-1} are attributed to the stretching vibration and in-plane

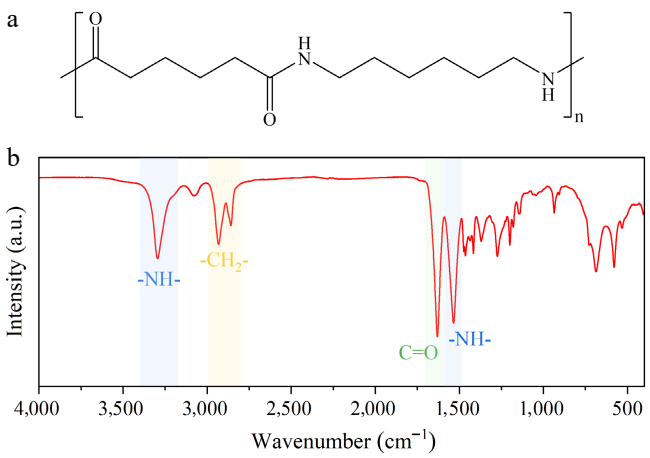

Fig. 1 (a) Chemical structure. (b) Infrared spectrum of nylon 6/6.

bending vibration of the –NH– group, respectively[24]. The peak at 1,634 cm^{-1} corresponds to the C=O stretching vibration of the amide group[19]. The stretching vibrations of aliphatic $–CH_2–$ are observed at 2,933 and 2,861 cm^{-1}.

TG-FTIR-GC/MS analysis

A TG-FTIR-GC/MS analyzer (TGA8000-Spectrum3-Clarus690-ClarusSQ8T, PerkinElmer, USA) was employed to investigate the pyrolysis characteristics of nylon 6/6. In the TG unit, the sample was heated to 800 °C at 20 °C/min under a high-purity nitrogen atmosphere (99.999%). The released volatiles were purged through a heated transfer line maintained at 280 °C into the FTIR spectrometer for online infrared analysis. FTIR detection was performed in the wavenumber range of 4,000–600 cm^{-1} with a resolution better than 0.4 cm^{-1}. When the sample's weight loss rate reached its maximum, the transfer channel was opened for 20 s to collect pyrolysis volatiles for offline GC/MS analysis. An Elite-5MS capillary column was used for separating the volatiles. The column temperature was initially held at 40 °C for 3 min, then increased at 10 °C/min to 280 °C and held for 3 min. The MS ion source utilized 70 eV electron ionization, with a quadrupole mass analyzer scanning the mass-to-charge ratio (m/z) range of 45–400. The acquired mass spectra were compared with the National Institute of Standards and Technology (NIST) 2017 database for volatile component identification, and the relative content of each compound was calculated using chromatographic peak area normalization.

Pyrolysis kinetics

Coats-Redfern integral and Achar differential methods were employed to calculate the pyrolysis kinetic parameters of nylon 6/6[25,26]. The corresponding equations are given as Eqs (1) and (2), respectively.

$$\ln\left[\frac{g(\alpha)}{T^2}\right] = \ln\left[\frac{AR}{\beta E_a}\right] - \frac{E_a}{RT} \quad (1)$$

$$\ln\left[\frac{d\alpha/dT}{f(\alpha)}\right] = \ln\left(\frac{A}{\beta}\right) - \frac{E_a}{RT} \quad (2)$$

where, $g(\alpha)$ and $f(\alpha)$ denote the integral and differential forms of the reaction model, respectively; T (K) is the absolute temperature; A (min^{-1}) denotes the pre-exponential factor; R (8.314 J/mol/K) represents the gas constant; β (°C/min) denotes the heating rate; E_a (kJ/mol) is the apparent activation energy; α represents the thermal conversion, defined as $\alpha = (m_i - m_t)/(m_i - m_f)$, where m_i, m_t, and m_f denote the initial, instantaneous, and final mass of the sample, respectively.

For the Coats-Redfern and Achar methods, straight lines were obtained by plotting $\ln[g(\alpha)/T^2]$ and $\ln[d\alpha/dT/f(\alpha)]$ against $1/T$, respectively. The apparent activation energy (E_a) and pre-exponential factor ($\ln A$) values were calculated from the slope and intercept. The most probable mechanism function was identified based on the following criteria: (i) $0 < E_a < 400$ kJ/mol; (ii) the E_a and lnA values calculated by the Coats-Redfern and Achar methods were in closest agreement; and (iii) a high linear correlation coefficient ($R^2 > 0.98$) was achieved[26].

Density functional theory calculations

All quantum chemical calculations were performed using the Gaussian 16 software package[27]. The geometric structure of the nylon 6/6 model molecule was fully optimized at the B3LYP/6-311G(d,p) level using density functional theory (DFT) method to identify the most thermodynamically stable conformer, which is essential for ensuring the reliability of subsequent calculations, as it represents the lowest-energy state and serves as the fundamental reference for reaction pathway analysis. Frequency calculations were subsequently conducted at the same level to confirm that the optimized structure corresponded to a true local minimum on the potential energy surface (no imaginary frequencies), thereby validating the absence of transition states or saddle points. The Cartesian coordinates of all atoms in the optimized model molecule are provided in Supplementary Table S1. The ESP was mapped onto the molecular van der Waals surface using GaussView software, where blue indicates the electropositive regions and red represents the electronegative regions.

For a quantitative assessment of the local reactivity, the Fukui function indices were calculated based on conceptual DFT. Single-point energies of the optimized model molecule were calculated in its neutral, cationic, and anionic states at the B3LYP/6-311G(d,p) level. Atomic charges were then extracted using Multiwfn program[28], and the nucleophilic attack index (f^+), electrophilic attack index (f^-), and radical attack index (f^0) were evaluated according to the following expressions[29]:

$$f^+ = q(N) - q(N+1) \quad (3)$$

$$f^- = q(N-1) - q(N) \quad (4)$$

$$f^0 = \frac{q(N-1) - q(N+1)}{2} \quad (5)$$

where, $q(N)$, $q(N+1)$, and $q(N-1)$ represent the atomic charges of the neutral, anionic, and cationic systems, respectively.

The BDE for a specific A–B bond in the nylon 6/6 model molecule was calculated to evaluate its thermal stability. The keyword 'Temperature = 753.15' was included in the frequency calculations to account for thermal corrections at the target temperature, which corresponds to the peak decomposition temperature (480 °C) of nylon 6/6 observed in the thermogravimetric analysis (Fig. 2), ensuring accurate enthalpy adjustments that reflect actual pyrolysis conditions. The structures of the model molecule and the two radical fragments (A• and B•) generated by homolytic cleavage were optimized at the B3LYP/6-311G(d,p) level, followed by frequency calculations to obtain the thermal corrections to enthalpy (H_{cor}). Subsequently, high-precision single-point energy (SPE) calculations were performed at the M06-2X/def2TZVP level, which provides significantly more reliable results than conventional functionals (e.g., B3LYP) with reasonable computational cost. The BDE was then computed by Eq. (6). This methodology and theoretical level are

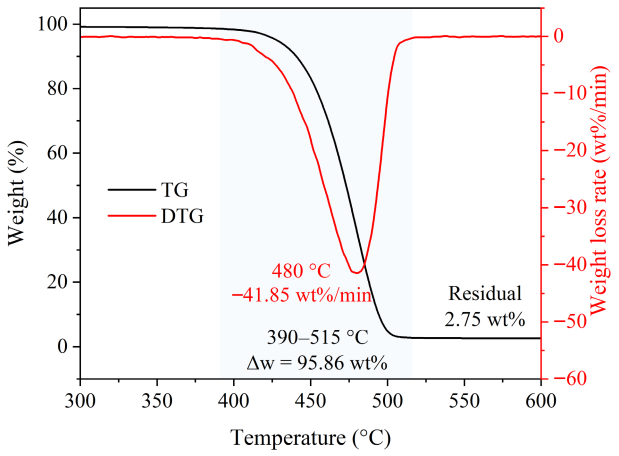

Fig. 2 TG and DTG curves of nylon 6/6.

https://doi.org/10.48130/prkm-0026-0014

well-documented in the literature for bond dissociation energy computations.

$$BDE = SPE(A\cdot) + H_{cor}(A\cdot) + SPE(B\cdot) + H_{cor}(B\cdot) - SPE(nylon6/6) - H_{cor}(nylon6/6) \quad (6)$$

Results and discussion

Pyrolysis behavior and kinetic analysis of nylon 6/6

Pyrolysis behavior

The pyrolysis behavior of nylon 6/6 at 20 °C/min was investigated by the thermogravimetric (TG) and derivative thermogravimetric (DTG) analyses, as depicted in Fig. 2. The primary pyrolysis stage occurs within the temperature range of 390–515 °C, accounting for a significant weight loss (Δw) of 95.86 wt%, which leaves a residual weight of merely 2.75 wt%. The high total weight loss observed here confirms the low thermal stability of the aliphatic polyamide structure at elevated temperatures, leading to near-complete volatilization. The maximum decomposition rate, as indicated by the distinct peak on the DTG curve, is –41.85 wt%/min at 480 °C. These results are in close agreement with the reported thermal degradation profiles of nylon polymers. For instance, a study by Wang et al.[19] reported the main decomposition stage for nylon 6 typically between 310 and 479 °C, with a peak mass loss rate occurring around 450 °C. Fundamentally, this pronounced single-step degradation is intrinsically linked to the cracking of amide linkages (–NH–CO–) within the polymer backbone. The narrow temperature range of the primary decomposition stage suggests a high degree of structural uniformity and a dominant, chain-reaction-like depolymerization pathway once initiated[30]. In short, the TG/DTG data provide a clear macroscopic reflection of the key structural evolution during the pyrolysis of nylon 6/6.

Apparent kinetic analysis

Based on the thermogravimetric data, the apparent pyrolysis kinetics of nylon 6/6 were investigated using the Coats-Redfern (integral) and Achar (differential) methods. A series of 19 common solid-state reaction mechanism functions were applied, encompassing chemical reaction models (F_1–F_5), diffusion models (D_1–D_4), nucleation and growth models ($A_{3/2}$–A_4), geometric contraction models (R_1–R_3), and power law models (P_2–P_4)[31]. Their respective integral and differential forms are listed in Supplementary Table S2. The calculated E_a, ln$A$, and R^2 values for various mechanism functions are summarized in Table 1.

Among all tested models, the first-order chemical reaction model (F_1) yields the most consistent parameters. Specifically, the E_a and ln$A$ values calculated via the Coats-Redfern (288 kJ/mol, 46.4 min^{-1}) and Achar (268 kJ/mol, 43.2 min^{-1}) methods are remarkably close. The linear fitting curves for the F_1 model are shown in Fig. 3. Notably, the minor deviations between the experimental data and the linear fits reflect the inherent challenges in modeling the complex pyrolysis kinetics. These deviations primarily arise because the simplified single-reaction assumption of the F_1 kinetic model cannot fully capture the multiple reactions and heat/mass transfer effects occurring during the actual degradation process of nylon 6/6[25]. Additionally, measurement sensitivities in experimental parameters such as sample mass and temperature introduce systematic errors. Nevertheless, the exceptionally high R^2 values above 0.99 indicate that the F_1 model can still adequately describe the main degradation stage of nylon 6/6. In contrast, the application of other mechanism functions leads to significantly different or even unrealistic results. For instance, diffusion-controlled models (D_1–D_4) yield much higher activation energies and inferior fits, while power law models (P_2–P_4) produce negative activation energies from the Achar method. The poor performance of these alternative models suggests they fail to capture the fundamental chemical nature of nylon 6/6 decomposition, which is not governed by diffusion limitations, interfacial reactions, or complex nucleation processes under the present conditions.

Consequently, the F_1 model is identified as the most probable mechanism function for the pyrolysis of nylon 6/6. This conclusion is strongly supported by the literature, where a first-order model is also predominantly reported for the thermal degradation of nylon 6, a closely related polyamide[23]. The consistency across different nylons underscores a universal degradation pathway primarily driven by the thermally induced scission of amide structures. The

Table 1. Kinetic analysis results using different mechanism functions.

Model code	Coats-Redfern			Achar		
	E_a (kJ/mol)	ln$A$ (min^{-1})	R^2	E_a (kJ/mol)	ln$A$ (min^{-1})	R^2
F_1	288	46.4	0.9905	268	43.2	0.9931
F_2	396	65.4	0.9296	428	71.0	0.8789
F_3	529	89.0	0.8195	587	98.7	0.7832
F_4	672	114.0	0.7428	746	126.5	0.7252
F_5	810	139.8	0.6932	905	154.2	0.6877
D_1	485	76.9	0.9480	358	55.2	0.7733
D_2	508	80.2	0.9612	410	63.6	0.8744
D_3	543	85.0	0.9784	493	76.6	0.9752
D_4	519	80.7	0.9672	440	67.4	0.9242
$A_{3/2}$	188	30.0	0.9890	169	26.8	0.9755
A_2	138	21.6	0.9884	110	18.5	0.9401
A_3	88	13.2	0.9872	69	10.1	0.8068
A_4	63	8.8	0.9859	44	5.8	0.6011
R_1	237	37.1	0.9453	110	15.5	0.3624
R_2	257	40.1	0.9692	189	28.7	0.8738
R_3	266	41.3	0.9773	216	32.9	0.9519
P_2	112	16.9	0.9391	-14	-4.7	0.0133
P_3	71	9.9	0.9320	-56	-11.6	0.1840
P_4	50	6.3	0.9236	-77	-15.2	0.3089

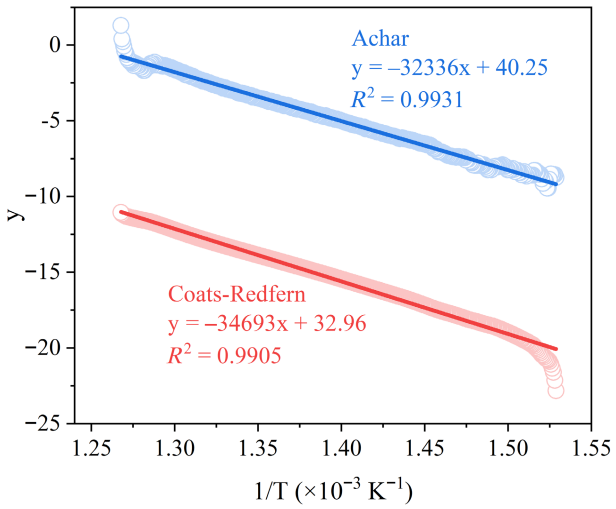

Fig. 3 Linear fitting curves using the F_1 kinetic model for nylon 6/6 pyrolysis.

sharp peak observed in the DTG curve corresponds macroscopically to this dominant, first-order depolymerization process. The average E_a and ln$A$, derived from the two methods, are 278 kJ/mol and 44.8 min^{-1}, respectively. These values are slightly higher than reported data for nylon 6 pyrolysis (228 kJ/mol and 36.4 min^{-1}), potentially attributable to the more ordered structure and stronger inter-chain hydrogen bonding in nylon 6/6[22].

Evolution of pyrolysis volatiles of nylon 6/6

Three-dimensional infrared spectrum analysis of volatiles

Online FTIR analysis was employed to monitor the release of characteristic functional groups and gas products during the thermal decomposition of nylon 6/6. The three-dimensional (3D) FTIR spectrum, depicting the absorbance as a function of temperature and wavenumber, along with its two-dimensional (2D) projection, is illustrated in Fig. 4. The volatile compounds attained their highest absorbance at approximately 480 °C, a temperature in agreement with the primary degradation peak of nylon 6/6 from the DTG analysis.

The prominent absorption peaks at 2,936 and 2,868 cm^{-1} were attributed to the asymmetric and symmetric C–H stretching vibrations of $–CH_2–$ groups, respectively[32]. These signals are characteristic of saturated methylene chains, likely originating from the cleavage of aliphatic segments in the nylon 6/6 backbone. A distinct peak at 2,360 cm^{-1}, characteristic of CO_2, demonstrates possible decarboxylation reactions[24]. The absorption at 1,766 cm^{-1}, assigned to C=O stretching vibrations, occurred at a higher wavenumber than typical amide carbonyl groups (near 1,640 cm^{-1}), implying the formation of non-amide carbonyl species such as ketones via secondary reactions[18]. The peak near 1,698 cm^{-1}, associated with C=C stretching vibrations of terminal alkenes ($–CH=CH_2$), further supports the cleavage of alkyl chains and the generation of unsaturated compounds. Additionally, the absorption at 1,502 cm^{-1} may arise from N–H bending vibrations, indicative of primary or secondary amines resulting from amide structure scission. Two sharp peaks at 964 and 930 cm^{-1}, identified as typical signatures of gaseous NH_3[23], highlight the deamination processes during pyrolysis. In short, the observed functional groups collectively reflect the complex degradation pathways of nylon 6/6. The release of methylene-rich fragments and CO_2 aligns with the breakdown of aliphatic segments and decarboxylation, while the formation of non-amide carbonyls and NH_3 underscores the role of amide bond cleavage and secondary reactions (such as cyclization and rearrangement). These insights demonstrate the key role of 3D FTIR analysis in elucidating the mechanistic details of nylon 6/6 pyrolysis.

Composition of pyrolysis volatiles based on GC/MS analysis

To identify the specific components of nylon 6/6 pyrolysis volatiles, offline GC/MS analysis was performed at the peak decomposition temperature of 480 °C. Presented in Fig. 5 is the total ion chromatogram (TIC). The primary peaks on the chromatogram are labeled to indicate the corresponding compound names, relative abundances, and structural formulas, with all match factors greater than 80%. A dominant peak at a retention time of 4.60 min was identified as cyclopentanone (CAS 120-92-3), exhibiting a high selectivity of 79.64%. This compound aligns with the FTIR-detected absorptions corresponding to saturated $–CH_2–$ groups and non-amide C=O stretching. Consequently, the formation of cyclopentanone is characteristic of nylon 6/6 pyrolysis, possibly arising from the cleavage of amide bonds adjacent to adipic acid segments, followed by intramolecular cyclization of the resulting diacid fragments. Another significant peak at 7.10 min was assigned to 1-amino-5-hexene (CAS 34825-70-2), which correlates with FTIR signals attributed to terminal alkenes, methylene chains, and N–H bending vibrations. This compound likely originates from the partial decomposition of hexamethylenediamine-derived segments, involving C–N bond cleavage near the imine group and the formation of an unsaturated terminal[22]. Its detection confirms the release of amine-containing volatiles, consistent with the observed NH_3 signatures resulting from deamination reactions. In summary, the integration of FTIR and GC/MS results offers a comprehensive understanding of the pyrolysis products of nylon 6/6. The strong agreement between the two techniques confirms that the thermal degradation proceeds through a combination of cleavage of amide groups, decarboxylation, deamination, and secondary rearrangement reactions, ultimately generating a mixture of cyclic ketones, unsaturated amines, and gaseous species such as CO_2 and NH_3.

Insights into backbone degradation mechanisms of nylon 6/6 based on DFT calculations

Detailed DFT calculations were performed to elucidate the backbone degradation mechanism of nylon 6/6 and correlate it with experimental data. Given the prohibitive computational cost associated with simulating the entire polymer chain, a minimum repeating unit of nylon 6/6, derived from the condensation of one molecule of hexamethylenediamine and one molecule of adipic

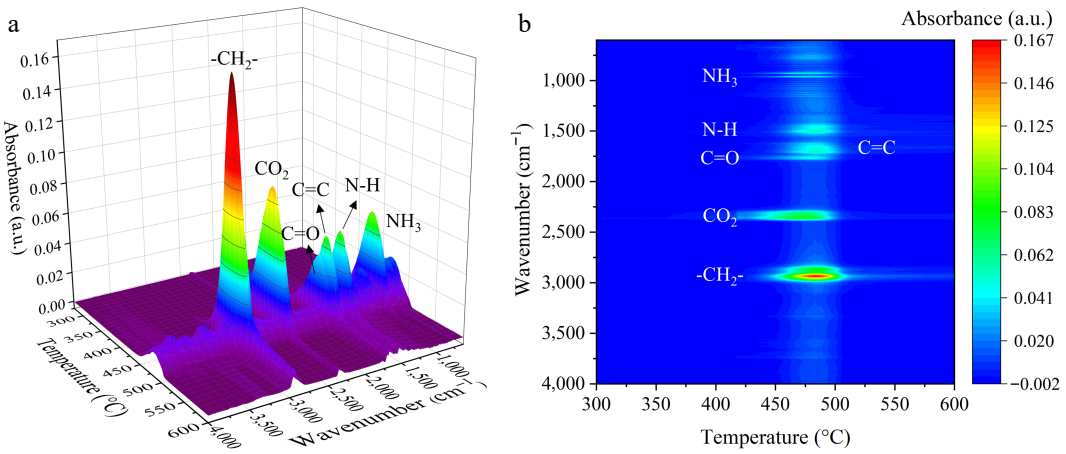

Fig. 4 (a) 3D FTIR spectrum. (b) Corresponding 2D projection of nylon 6/6 pyrolysis volatiles.

https://doi.org/10.48130/prkm-0026-0014

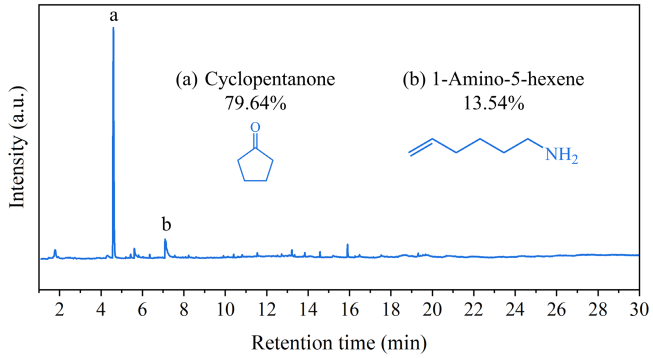

Fig. 5 GC/MS analysis results of nylon 6/6 pyrolysis volatiles.

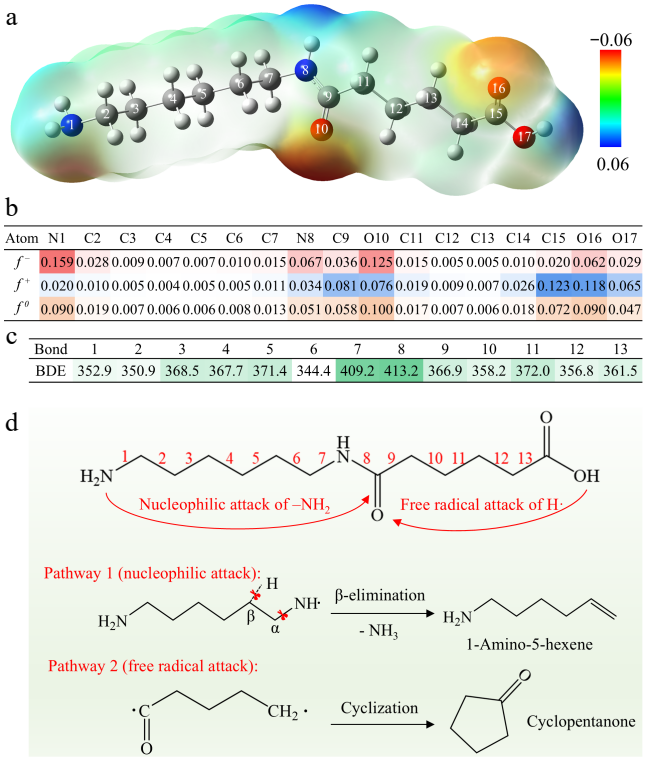

Fig. 6 (a) Electrostatic potential (ESP)-mapped surface of nylon 6/6 model molecule. (b) Fukui functions of key atom sites. (c) Bond dissociation energies (BDEs) of backbone chemical bonds. (d) Two possible decomposition pathways of the nylon 6/6 model molecule.

acid, was constructed as the model molecule (Fig. 6a). The model retains active amino and carboxyl terminal groups, accurately representing the ends of a real polymer chain. Key atoms in the backbone are numerically labeled for clear reference in subsequent analyses.

The ESP distribution mapped onto the van der Waals surface of the optimized model molecule is presented in Fig. 6a. The color gradient, from blue (most positive/electron-poor regions) to red (most negative/electron-rich regions), visually reveals the charge distribution. Notably, within the amide linkage, the carbonyl oxygen atom (O10) exhibits a pronounced red hue, indicating a region of high electron density (partial negative charge). In contrast, the hydrogen atom bonded to the amide nitrogen (N8) resides in a blue zone, signifying a partial positive charge. This polarization arises from the combined effect of the high electronegativity of the oxygen atom and the p-π conjugation within the amide group, which delocalizes the lone pair electrons from the nitrogen atom towards the carbonyl group[30]. This charge separation is fundamental for the formation of strong intermolecular hydrogen bonds in the solid state, where the carbonyl oxygen of one chain interacts with the imine hydrogen of an adjacent chain. The resulting dense and regular hydrogen-bonding network in nylon 6/6, facilitated by its symmetrical and extended chain structure, contributes significantly to its high mechanical strength, wear resistance, and thermal stability[33]. The energy required to disrupt this ordered structure and initiate degradation is consequently high. This provides a microscopic explanation for the higher apparent pyrolysis activation energy of nylon 6/6 (278 kJ/mol) compared to the literature-reported value for nylon 6 (228 kJ/mol), which possesses a less symmetric amide structure and weaker hydrogen bonding[23].

The detection of CO_2, NH_3, cyclopentanone, and 1-amino-5-hexene via FTIR and GC/MS points towards the decomposition of the amide structure. To investigate the specific bond cleavage sequences and formation pathways of these characteristic products, the condensed Fukui functions (f^-, f^+, and f^0) for key atoms and the BDEs for critical bonds in the model molecule were calculated, as summarized in Fig. 6b and c, respectively. The corresponding chemical bonds are labeled with numerical indices, as illustrated in Fig. 6d. The BDE analysis reveals that the C-N bonds within and adjacent to the amide group (Bonds 8 and 7) possess the highest dissociation energies (413.2 and 409.2 kJ/mol, respectively). This exceptional stability is a direct consequence of the p-π conjugation of the amide structure and its long-range delocalization effects, a fact corroborated by the shortened C-N bond length in the optimized geometry (Fig. 6a). The high BDEs suggest that simple homolytic cleavage of these bonds is thermodynamically unfavorable at the onset of pyrolysis. Moreover, the BDE of the amide C–N bond obtained from DFT calculations is markedly higher than the apparent pyrolysis activation energy of nylon 6/6. In practice, the activation energy denotes a collective energy barrier that includes phase transitions, hydrogen bond dissociation, and chemical bond cleavage[20]. The numerical discrepancy indicates that the thermal degradation of nylon 6/6 is not predominantly initiated by direct C–N bond scission; rather, it is more likely to proceed via pathways such as chain-radical reactions triggered by terminal active groups, which significantly lower the apparent activation energy. The condensed Fukui functions provide insights into the susceptibility of atomic sites to different types of attacks (Fig. 6b). The highest f^- value (0.159) of the terminal amino nitrogen atom (N1) indicates its strongest nucleophilicity. This aligns with the ESP map, which shows a pronounced electron-rich (red) region around N1. Conversely, the f^+ function, marking electrophilic attack sites, is highest for the carbonyl carbon and oxygen (C15 and O16) of the terminal carboxyl group and second-highest for the C9 and O10 atoms of the amide group. The amide oxygen atom (O10) also exhibits the highest f^0 value, representing susceptibility to radical attack[29].

Integrating these computational indicators allows for the proposal of two possible initial degradation pathways of the nylon 6/6 model molecule, as illustrated in Fig. 6d. In Pathway 1, the electron-rich terminal amino group (–NH_2 at N1) acts as an intramolecular nucleophile, attacking the adjacent amide group with electrophilic sites (C9 and O10). This nucleophilic addition disrupts the amide resonance, weakens the C-N bond (Bond 8), and leads to its cleavage[30]. The generated amino radical is highly reactive, such that it tends to abstract the hydrogen atom attached to the β-carbon, leading to β-elimination to form a C=C bond with concomitant release of NH_3[22]. This deamination process aligns with

GC/MS detection of 1-amino-5-hexene and FTIR observation of NH_3 release. In Pathway 2, decarboxylation of the terminal carboxyl group, suggested by the CO_2 release observed by FTIR, could generate hydrogen radicals. The highest f^0 value (0.100) of the amide oxygen (O10) identifies it as the preferred site for radical attack. Hydrogen radical addition to the carbonyl oxygen can weaken the amide linkage, leading to the homolytic scission of the C–N bond (Bond 8). The resulting adipic acid segment then undergoes intramolecular cyclization to form cyclopentanone, consistent with its high selectivity (79.64%) in GC/MS analysis. Both pathways are theoretically supported by DFT calculations: pathway 1 correlates with the high nucleophilicity of N1, while Pathway 2 leverages the radical susceptibility of O10 and the high BDE of Bond 8, which necessitates alternative activation mechanisms over direct homolysis.

In summary, the DFT calculations provide a crucial micro-mechanistic framework that corroborates the macro-scale experimental observations. The high stability of the amide C–N bond, as evidenced by its high BDE, directs the initial pyrolysis reactions towards alternative pathways involving nucleophilic or radical attacks at specific sites identified by Fukui function analysis. Pathway 1 rationalizes the formation of NH_3 and 1-amino-5-hexene via intramolecular ammonolysis, while Pathway 2 accounts for the formation of CO_2 and cyclopentanone via a radical-mediated mechanism followed by cyclization. This synergy between theoretical simulation and experimental method offers profound insights into the complex pyrolysis mechanism of nylon 6/6, providing essential guidance for controlling its pyrolysis towards desired product distributions.

Conclusions

By coupling TG-FTIR-GC/MS and DFT calculations, this work explores the pyrolysis kinetics, volatile evolution, and backbone degradation pathways of nylon 6/6. The thermal degradation of nylon 6/6 results in a substantial weight loss of 95.86 wt% between 390 and 515 °C, exhibiting a sharp pyrolysis peak at 480 °C. The pyrolysis process follows the first-order chemical reaction model, with an activation energy determined to be 278 kJ/mol.

The released characteristic functional groups during pyrolysis include methylene chains, terminal alkenes, carbonyl groups, CO_2, and NH_3. The primary volatile products were identified as cyclopentanone (79.64%) and 1-amino-5-hexene (13.54%). With a high BDE of 413.2 kJ/mol, the direct homolytic cleavage of the amide C–N bond in the nylon 6/6 model molecule is thermodynamically unfavorable. Instead, two possible reaction pathways are proposed: nucleophilic attack by the terminal amino group and radical attack by H• at the amide carbonyl. Both pathways cleave the amide C–N bond, yielding hexamethylenediamine and adipic acid segments. These intermediates then undergo deamination and cyclization reactions, ultimately producing 1-amino-5-hexene and cyclopentanone, respectively. By integrating experimental analysis with theoretical calculations, this work elucidates the pyrolysis mechanism of nylon 6/6 in depth, thereby offering a scientific basis for its efficient thermal conversion and recovery.

Author contributions

The authors confirm contribution to the paper as follows: study conception and design, validation: Chen Y; methodology: Xiao H, Wang X, Yang H; investigation: Xu D, Feng S; formal analysis, data curation, visualization, and draft manuscript preparation: Xu D; resources: Chen H; writing – review and editing: Xiao H, Yang H; supervision: Chen H, Yang H; funding acquisition: Yang H. All authors reviewed the results and approved the final version of the manuscript.

Data availability

All data generated or analyzed during this study are included in this published article.

Acknowledgments

The authors wish to express sincere thanks for the financial support from the Key Program of National Natural Science Foundation of China (Grant No. 52436007), National Key Research and Development Program of China (Grant No. 2024YFC3909204), and National Science Fund for Distinguished Young Scholars (Grant No. 52125601). The authors are also grateful for the assistance on the product analysis provided by the Analytical and Testing Center at Huazhong University of Science & Technology (http://atc.hust.edu.cn), Wuhan 430074, China.

Conflict of interest

The authors declare that they have no conflict of interest.

Supplementary information accompanies this paper online at: https://doi.org/10.48130/prkm-0026-0014.

Dates

Received 10 December 2025; Revised 8 April 2026; Accepted 13 May 2026; Published online 31 July 2026

References

[1] Zhang X, She Y, Wen X, Hu G, Yu X, et al. 2026. Upcycling waste plastic into electrocatalyst: waste nylon fishnet-derived flexible & rigid Co/Fe-MOF for efficient oxygen evolution reaction. *Applied Catalysis B: Environment and Energy* 384:126184

[2] Yang W, Jung S, Lee J, Lee SW, Kim YT, et al. 2023. Selective recovery of caprolactam from the thermo-catalytic conversion of textile waste over γ-Al_2O_3 supported metal catalysts. *Environmental Pollution* 329:121684

[3] Liu Z, Yang Y, Xie M, Cheng M, Yang R, et al. 2024. TG-FTIR-Py-GCMS analysis and catalytic pyrolysis mechanism of textile waste by red mud catalyst for liquid fuel production. *Science of the Total Environment* 952:175874

[4] Conk RJ, Stahler JF, Shi JX, Yang J, Lefton NG, et al. 2024. Polyolefin waste to light olefins with ethylene and base-metal heterogeneous catalysts. *Science* 385:1322–1327

[5] Cai N, Jia S, Sun K, Zhu J, Zhao C, et al. 2025. High-Value utilization of waste plastics: transforming plastic polymers into thin-walled and uniform carbon nanotubes via catalytic pyrolysis. *Green Energy & Environment*

[6] Xiao H, Harding J, Lei S, Chen W, Xia S, et al. 2022. Hydrogen and aromatics recovery through plasma-catalytic pyrolysis of waste polypropylene. *Journal of Cleaner Production* 350:131467

[7] Xiao H, Li S, Shi Z, Cui C, Xia S, et al. 2023. Plasma-catalytic pyrolysis of polypropylene for hydrogen and carbon nanotubes: understanding the influence of plasma on volatiles. *Applied Energy* 351:121848

[8] Munyaneza NE, Ji R, DiMarco A, Miscall J, Stanley L, et al. 2024. Chain-length-controllable upcycling of polyolefins to sulfate detergents. *Nature Sustainability* 7:1681–1690

https://doi.org/10.48130/prkm-0026-0014

[9] Sukkasem T, Yoojaroen N, Truadnog Y, Prayutte P, Junpirom S, et al. 2026. Converting polystyrene waste into valuable oils: high performance of SUZ-4 zeolite for selective oil component conversion in catalytic pyrolysis. *Fuel* 405:136456
[10] Wang Z, Shen J, Liu X, Guo Y, Wang S, et al. 2023. A review on nitrogen migration mechanism during the pyrolysis of organic solid waste: DFT, ReaxFF MD and experimental study. *Journal of Analytical and Applied Pyrolysis* 176:106250
[11] Wang P, Qiao L, Wang W, Yu J, Millan M. 2023. The behavior of heteroatom compounds during the pyrolysis of waste composite plastics. *Journal of Analytical and Applied Pyrolysis* 173:106080
[12] de Rezende Locatel W, Mohabeer C, Laurenti D, Schuurman Y, Guilhaume N. 2022. Co-pyrolysis of beech wood and polyamide-6: impact of plastic concentration and wood/plastic synergistic effects. *Journal of Analytical and Applied Pyrolysis* 168:105779
[13] de Rezende Locatel W, Mohabeer C, Laurenti D, Schuurman Y, Guilhaume N. 2022. Co-pyrolysis of beech wood and polyamide-6: effect of HZSM-5 catalyst on the properties of pyrolysis oils. *Journal of Analytical and Applied Pyrolysis* 167:105696
[14] Kumagai S, Hosaka T, Kameda T, Yoshioka T. 2015. Steam pyrolysis of polyimides: effects of steam on raw material recovery. *Environmental Science & Technology* 49:13558−13565
[15] Kumar A, von Wolff N, Rauch M, Zou YQ, Shmul G, et al. 2020. Hydrogenative depolymerization of nylons. *Journal of the American Chemical Society* 142:14267−14275
[16] Chen G, Liu T, Luan P, Li N, Sun Y, et al. 2023. Distribution, migration, and removal of N-containing products during polyurethane pyrolysis: a review. *Journal of Hazardous Materials* 453:131406
[17] Zheng B, Li Y, Ma H, Chen G, Gu Y, et al. 2024. Pyrolysis characteristics, kinetics and products of flexible polyurethane foam in luxury cruise ship via TG, FTIR, GC-MS and Shuffled Complex Evolution. *Journal of Analytical and Applied Pyrolysis* 179:106497
[18] Xu D, Lin J, Sun S, Ma R, Wang M, et al. 2022. Microwave pyrolysis of biomass model compounds for bio-oil: formation mechanisms of the nitrogenous chemicals and DFT calculations. *Energy Conversion and Management* 262:115676
[19] Wang G, Zhang Z, Xu D, Xing B, Zhu L, et al. 2023. Insight into pyrolysis mechanism of plastic waste with C-O/C-N bonds in the backbone. *Science of the Total Environment* 897:165359
[20] Xuan W, Yan S, Dong Y. 2023. Exploration of pyrolysis behaviors of waste plastics (polypropylene plastic/polyethylene plastic/polystyrene plastic): macro-thermal kinetics and micro-pyrolysis mechanism. *Processes* 11:2764
[21] Huang J, Meng H, Luo X, Mu X, Xu W, et al. 2022. Insights into the thermal degradation mechanisms of polyethylene terephthalate dimer using DFT method. *Chemosphere* 291:133112
[22] Zheng Z, Yao JL, Yao Q. 2024. Thermal degradation of polyamide 66 and its model compound. *Polymer Degradation and Stability* 228:110909
[23] Xu D, Wei Y, Xiao H, Zhang T, Sheng Z, et al. 2026. Pyrolysis kinetics, volatile evolution, and backbone degradation mechanisms of typical nitrogen-containing plastics based on TG-FTIR-GC/MS and density functional theory. *Journal of Analytical and Applied Pyrolysis* 193:107418
[24] Xu D, Lin J, Ma R, Hou J, Sun S, et al. 2023. Fast pyrolysis of algae model compounds for bio-oil: in-depth insights into the volatile interaction mechanisms based on DFT calculations. *Fuel* 333:126449
[25] Wei P, Chen G, Zhi F, Zhang A, Deng H, et al. 2024. Investigation of pyrolysis and combustion characteristics of chili straw waste with different O2/N2 ratios and heating rates. *Thermochimica Acta* 742:179875
[26] Wu C, Ge S, Li J, Shi B, Wang Y, et al. 2023. The effect of N_2/CO_2 blend ratios on the pyrolysis and combustion behaviors of coal particles: kinetic and thermodynamic analyses. *Journal of Loss Prevention in the Process Industries* 84:105120
[27] Frisch MJ, Trucks GW, Schlegel HB, Scuseria GE, Robb MA, et al. 2016. Gaussian 16 Rev. C. 01. Wallingford, CT
[28] Lu T, Chen F. 2011. Multiwfn: a multifunctional wavefunction analyzer. *Journal of Computational Chemistry* 33:580−592
[29] Qu W, Chen C, Tang Z, Xia D, Ma D, et al. 2022. Electron-rich/poor reaction sites enable ultrafast confining Fenton-like processes in facet-engineered BiOI membranes for water purification. *Applied Catalysis B: Environmental* 304:120970
[30] Didovets Y, Brela MZ. 2022. Theoretical study on the thermal degradation process of nylon 6 and polyhydroxybutyrate. *Physchem* 2:334−346
[31] Luo M, Shao S, Cao Y, Li X, Wu S. 2025. A study on the characteristics and kinetic of co-catalytic pyrolysis with rape straw and ABS waste plastics. *Renewable Energy* 242:122450
[32] Zhang L, Zhou N, Ke L, Zeng Y, Wu Q, et al. 2025. Understanding the role of plastic additives in the pyrolysis of plastic wastes: impact of additives on product selectivity, kinetics, and mechanistic pathways. *Chemical Engineering Journal* 514:163194
[33] Chen R, Song X, in't Veld PJ, Luo C. 2025. Crystallization and heterogeneous local stress distribution in hydrogen-bonded polymers: molecular dynamics simulations of polyamide 6 (PA6). *Macromolecules* 58:424−438